AIAA JOURNAL
Vol. 38, No. 9, September 2000

# Numerically Consistent Strong Conservation Grid Motion for Finite Difference Schemes

R. Hixon*
*NASA John H. Glenn Research Center at Lewis Field, Cleveland, Ohio 44135*

**An investigation into the numerical issues of curvilinear coordinate grid motion for finite difference schemes is performed. Several formulations of the time-dependent curvilinear coordinate equations are compared using unsteady benchmark test problems. A new, numerically consistent method of computing the unsteady grid metrics for the strong conservation equations is developed and demonstrated.**

## Introduction

THE goal of computational fluid dynamics is to obtain accurate steady or unsteady flowfields about realistic geometries. To accomplish this goal, a spatial differencing scheme is combined with a time-marching method to advance the solution through time. One method of obtaining spatial differences is by the use of finite differences. Usually, finite differencing schemes are derived for uniformly spaced grids in Cartesian coordinates for computational simplicity and accuracy. However, applying such schemes to realistic flows with complex wall geometries can result in boundary conditions that are not easily implemented due to the irregularity that these geometries impose on the grid near the wall. Transforming the equations of motion from Cartesian coordinates to generalized curvilinear coordinates allows the use of stretched, body-fitted grids, thus simplifying the application of boundary conditions.

It is desirable, however, to allow the grid to adapt to the changing flow features and accuracy requirements as a realistic flow evolves. This allows both a more accurate solution as well as a more efficient solver that is less dependent on the initial grid generation.

To ensure that the finite difference scheme will numerically conserve mass, momentum, and energy, it is desirable to write the curvilinear equations in strong conservation form.[1] However, in the past it was soon recognized that the finite difference approximation to the three-dimensional strong conservation equations introduced errors due to the differencing used for the grid metrics.[2] Also, in using the strong conservation form of the governing equations on moving grids, problems with the time-varying transformation have required another equation to be solved to track the change in volume of the grid cells.[3]

However, there are several forms of the governing equations other than the strong conservation form that result from the transformation to generalized coordinates, and it is not certain which form of the equations is most accurate from a numerical standpoint. Hindman[4] tested various forms of the two-dimensional governing equations using a MacCormack scheme and found that the nonconservative chain-rule form of the equations was accurate even for nonlinear shock-capturing problems. Hixon et al.[5] tested four forms of the three-dimensional governing equations using a high-accuracy dispersion-relation-preserving (DRP) method[6] and also found that the strong conservation form of the equations was very inaccurate due to the numerical inconsistency of the grid metrics.

However, Thomas and Lombard[3] had derived grid metrics for stationary grids that were analytically equivalent but numerically consistent, and these metrics were tested using a sixth-order compact scheme by Gaitonde and Visbal.[7] These revised metrics were found to be very accurate, eliminating the grid metric problem for central differencing schemes on stationary grids.

For moving grids, however, the unsteady grid metrics are still not consistent. In this work, a new form of the Jacobian and the unsteady grid metrics are derived that are numerically consistent. These new metrics are used in the strong conservation equations and are tested against the chain rule form of the equations and the strong conservation form using the standard grid metrics.

## Governing Equations

The governing equations used in this work are the nonlinear three-dimensional Euler equations written in conservative form. In Cartesian coordinates, the Euler equations are

$$Q_t + E_x + F_y + G_z = 0 \tag{1}$$

where

$$Q = \begin{Bmatrix} \rho \\ \rho u \\ \rho v \\ \rho w \\ E \end{Bmatrix} \tag{2}$$

$$E = \begin{Bmatrix} \rho u \\ \rho u^2 + p \\ \rho uv \\ \rho uw \\ u(E + p) \end{Bmatrix}, \qquad F = \begin{Bmatrix} \rho v \\ \rho uv \\ \rho v^2 + p \\ \rho vw \\ v(E + p) \end{Bmatrix}$$

$$G = \begin{Bmatrix} \rho w \\ \rho uw \\ \rho vw \\ \rho w^2 + p \\ w(E + p) \end{Bmatrix} \tag{3}$$

Here

$$p = (\gamma - 1)\left[E - \tfrac{1}{2}\rho(u^2 + v^2 + w^2)\right] \tag{4}$$

and $\gamma$ is the ratio of specific heats, taken as 1.4 in this work.

## Generalized Curvilinear Coordinate Transformations

The coordinate transformations given here sketches the full derivation given by Pulliam,[8] following Vinokur.[1] The Euler equations can be transformed from Cartesian coordinates into generalized coordinates, where

$$\tau = t, \qquad \xi = \xi(x, y, z, t)$$
$$\eta = \eta(x, y, z, t), \qquad \zeta = \zeta(x, y, z, t) \tag{5}$$

Received 25 May 1999; revision received 22 January 2000; accepted for publication 17 February 2000. Copyright © 2000 by the American Institute of Aeronautics and Astronautics, Inc. No copyright is asserted in the United States under Title 17, U.S. Code. The U.S. Government has a royalty-free license to exercise all rights under the copyright claimed herein for Governmental purposes. All other rights are reserved by the copyright owner.

*Senior Research Associate, Institute for Computational Mechanics in Propulsion. Member AIAA.

Because $\tau = t$, from this point on $t$ will be used exclusively. Chain-rule expansions are used to represent the Cartesian derivatives in terms of the curvilinear derivatives

$$\begin{bmatrix} \partial_t \\ \partial_x \\ \partial_y \\ \partial_z \end{bmatrix} = \begin{bmatrix} 1 & \xi_t & \eta_t & \zeta_t \\ 0 & \xi_x & \eta_x & \zeta_x \\ 0 & \xi_y & \eta_y & \zeta_y \\ 0 & \xi_z & \eta_z & \zeta_z \end{bmatrix} \begin{bmatrix} \partial_t \\ \partial_\xi \\ \partial_\eta \\ \partial_\zeta \end{bmatrix} \tag{6}$$

Solving for the metric relations, we obtain

$$\begin{aligned} 1/J &= x_\xi y_\eta z_\zeta + x_\zeta y_\xi z_\eta + x_\eta y_\zeta z_\xi - x_\xi y_\zeta z_\eta - x_\eta y_\xi z_\zeta - x_\zeta y_\eta z_\xi \\ \xi_x/J &= y_\eta z_\zeta - y_\zeta z_\eta, \qquad \xi_y/J = x_\zeta z_\eta - x_\eta z_\zeta \\ \xi_z/J &= x_\eta y_\zeta - x_\zeta y_\eta \\ \xi_t/J &= -x_t(\xi_x/J) - y_t(\xi_y/J) - z_t(\xi_z/J) \\ \eta_x/J &= y_\zeta z_\xi - y_\xi z_\zeta, \qquad \eta_y/J = x_\xi z_\zeta - x_\zeta z_\xi \\ \eta_z/J &= x_\zeta y_\xi - x_\xi y_\zeta \\ \eta_t/J &= -x_t(\eta_x/J) - y_t(\eta_y/J) - z_t(\eta_z/J) \\ \zeta_x/J &= y_\xi z_\eta - y_\eta z_\xi, \qquad \zeta_y/J = x_\eta z_\xi - x_\xi z_\eta \\ \zeta_z/J &= x_\xi y_\eta - x_\eta y_\xi \\ \zeta_t/J &= -x_t(\zeta_x/J) - y_t(\zeta_y/J) - z_t(\zeta_z/J) \end{aligned} \tag{7}$$

Applying Eq. (6) to Eq. (1) results in the chain-rule form of the curvilinear equations:

$$\begin{aligned} &Q_t + \xi_t Q_\xi + \eta_t Q_\eta + \zeta_t Q_\zeta + \xi_x E_\xi + \eta_x E_\eta + \zeta_x E_\zeta \\ &\quad + \xi_y F_\xi + \eta_y F_\eta + \zeta_y F_\zeta + \xi_z G_\xi + \eta_z G_\eta + \zeta_z G_\zeta = 0 \end{aligned} \tag{8}$$

The chain rule form of the curvilinear equations are in a weak conservation form. To derive the strong conservation form, Eq. (8) is divided by the Jacobian $J$ and the product rule is applied. For example,

$$\xi_x/J(E)_\xi = [(\xi_x/J)E]_\xi - E(\xi_x/J)_\xi \tag{9}$$

When we apply this transformation, Eq. (8) becomes

$$\begin{aligned} &\left(\frac{Q}{J}\right)_t + \left(\frac{\xi_t}{J}Q + \frac{\xi_x}{J}E + \frac{\xi_y}{J}F + \frac{\xi_z}{J}G\right)_\xi \\ &\quad + \left(\frac{\eta_t}{J}Q + \frac{\eta_x}{J}E + \frac{\eta_y}{J}F + \frac{\eta_z}{J}G\right)_\eta \\ &\quad + \left(\frac{\zeta_t}{J}Q + \frac{\zeta_x}{J}E + \frac{\zeta_y}{J}F + \frac{\zeta_z}{J}G\right)_\zeta \\ &\quad - Q\left[\left(\frac{1}{J}\right)_t + \left(\frac{\xi_t}{J}\right)_\xi + \left(\frac{\eta_t}{J}\right)_\eta + \left(\frac{\zeta_t}{J}\right)_\zeta\right] \\ &\quad - E\left[\left(\frac{\xi_x}{J}\right)_\xi + \left(\frac{\eta_x}{J}\right)_\eta + \left(\frac{\zeta_x}{J}\right)_\zeta\right] \\ &\quad - F\left[\left(\frac{\xi_y}{J}\right)_\xi + \left(\frac{\eta_y}{J}\right)_\eta + \left(\frac{\zeta_y}{J}\right)_\zeta\right] \\ &\quad - G\left[\left(\frac{\xi_z}{J}\right)_\xi + \left(\frac{\eta_z}{J}\right)_\eta + \left(\frac{\zeta_z}{J}\right)_\zeta\right] = 0 \end{aligned} \tag{10}$$

The terms in brackets in Eq. (10) are known as the metric invariants of the transformation. If the equations for the metric relations are substituted into Eq. (10), the metric invariants of the transformation prove analytically to be zero. If they are discarded, the strong conservation form of the governing equations results:

$$\begin{aligned} &\left(\frac{Q}{J}\right)_t + \left[\left(\frac{\xi_t}{J}\right)Q + \left(\frac{\xi_x}{J}\right)E + \left(\frac{\xi_y}{J}\right)F + \left(\frac{\xi_z}{J}\right)G\right]_\xi \\ &\quad + \left[\left(\frac{\eta_t}{J}\right)Q + \left(\frac{\eta_x}{J}\right)E + \left(\frac{\eta_y}{J}\right)F + \left(\frac{\eta_z}{J}\right)G\right]_\eta \\ &\quad + \left[\left(\frac{\zeta_t}{J}\right)Q + \left(\frac{\zeta_x}{J}\right)E + \left(\frac{\zeta_y}{J}\right)F + \left(\frac{\zeta_z}{J}\right)G\right]_\zeta = 0 \end{aligned} \tag{11}$$

## Performance of Finite Difference Schemes

It is important to remember when using finite difference schemes to solve differential equations that the rules of differentiation that are analytically true are not necessarily numerically true for the discretized equation. For example, let us consider the product rule

$$(xy)_\xi - [x(y)_\xi + y(x)_\xi] = 0 \tag{12}$$

Analytically, this is true. However, if we define an explicit finite difference derivative in the $\xi$ direction as

$$\left(x^n_{i,j}\right)_\xi = \sum_{k=k_s}^{k_e} a_k x^n_{i+k,j} \tag{13}$$

where $i$ and $j$ denote the $\xi$ and $\eta$ grid point location and $n$ denotes the time level, we can substitute into Eq. (12) to find

$$\sum_{k=k_s}^{k_e} a_k x^n_{i+k,j} y^n_{i+k,j} - \left(x^n_{i,j} \sum_{k=k_s}^{k_e} a_k y^n_{i+k,j} + y^n_{i,j} \sum_{k=k_s}^{k_e} a_k x^n_{i+k,j}\right) \neq 0 \tag{14}$$

Thus, the product rule is not numerically true.

Some analytic rules are true numerically. For example, let us define a derivative in the $\eta$ direction as

$$\left(x^n_{i,j}\right)_\eta = \sum_{l=l_s}^{l_e} b_l x^n_{i,j+l} \tag{15}$$

Note that this difference is not necessarily the same as the differencing used in the $\xi$ direction. Using Eqs. (13) and (15), we find

$$\begin{aligned} \left[\left(x^n_{i,j}\right)_\xi\right]_\eta &= \sum_{l=l_s}^{l_e} b_l \left(\sum_{k=k_s}^{k_e} a_k x^n_{i+k,j+l}\right) \\ &= \sum_{l=l_s}^{l_e} \sum_{k=k_s}^{k_e} b_l a_k x^n_{i+k,j+l} \\ &= \sum_{k=k_s}^{k_e} \sum_{l=l_s}^{l_e} a_k b_l x^n_{i+k,j+l} \\ &= \left[\left(x^n_{i,j}\right)_\eta\right]_\xi \end{aligned} \tag{16}$$

Note, however, that there are conditions where this may not work. For example, if the $\xi$ derivative stencil had an $\eta$ dependence, such as with a stencil-shifting essentially nonoscillatory scheme, Eq. (16) would not be true. However, if the $\xi$ derivative stencil is changing in the $\xi$ direction only, such as at a boundary edge, Eq. (16) still holds.

Similarly, if we define a time derivative (or a stage of a Runge–Kutta method) as

$$\left(x^n_{i,j}\right)_t = \sum_{m=m_s}^{m_e} c_m x^{n+m}_{i,j} \tag{17}$$

it is apparent from Eq. (16) that

$$\left[\left(x^n_{i,j}\right)_t\right]_\xi = \left[\left(x^n_{i,j}\right)_\xi\right]_t \tag{18}$$

Another analytic rule that is true numerically for finite differencing is

$$(x + y)_\xi = (x)_\xi + (y)_\xi \tag{19}$$

Although it is not shown in this work, the same rules apply to compact differencing schemes as well. The validity of these rules becomes important when using the strong conservation form of the governing equations.

## Steady Metrics for the Strong Conservation Equations

As pointed out by Pulliam and Steger,[2] if the invariants of the transformation in Eq. (10) are computed using central differencing, the numerical result is not zero. Thus, for a finite difference method applied to Eq. (11), a uniform mean flow will not necessarily be recovered due to numerical inconsistencies with the grid metrics used. For example, the second metric invariant in Eq. (10) becomes

$$[(\xi_x/J)_\xi + (\eta_x/J)_\eta + (\zeta_x/J)_\zeta] = [(y_\eta z_\zeta)_\xi - (y_\zeta z_\eta)_\xi + (y_\zeta z_\xi)_\eta - (y_\xi z_\zeta)_\eta + (y_\xi z_\eta)_\zeta - (y_\eta z_\xi)_\zeta] \neq 0 \tag{20}$$

due to the numerical failure of the product rule.

To overcome this problem, Thomas and Lombard[3] pointed out that the metrics could be rewritten in this analytically identical form:

$$\begin{aligned}
\xi_x/J &= (y_\eta z)_\zeta - (y_\zeta z)_\eta, & \xi_y/J &= (x_\zeta z)_\eta - (x_\eta z)_\zeta \\
\xi_z/J &= (x_\eta y)_\zeta - (x_\zeta y)_\eta, & \eta_x/J &= (y_\zeta z)_\xi - (y_\xi z)_\zeta \\
\eta_y/J &= (x_\xi z)_\zeta - (x_\zeta z)_\xi, & \eta_z/J &= (x_\zeta y)_\xi - (x_\xi y)_\zeta \\
\zeta_x/J &= (y_\xi z)_\eta - (y_\eta z)_\xi, & \zeta_y/J &= (x_\eta z)_\xi - (x_\xi z)_\eta \\
\zeta_z/J &= (x_\xi y)_\eta - (x_\eta y)_\xi
\end{aligned} \tag{21}$$

Thus, for example, the second metric invariant in Eq. (10) becomes

$$[(\xi_x/J)_\xi + (\eta_x/J)_\eta + (\zeta_x/J)_\zeta] = [(y_\eta z)_{\zeta\xi} - (y_\zeta z)_{\eta\xi} + (y_\zeta z)_{\xi\eta} - (y_\xi z)_{\zeta\eta} + (y_\xi z)_{\eta\zeta} - (y_\eta z)_{\xi\zeta}] = 0 \tag{22}$$

because the order of differentiation can be interchanged numerically as shown in Eq. (16).

Note that, for this method to work, all metric derivatives must be computed using the same differencing stencils that are used for the flux derivatives. For example, a MacCormack scheme uses a forward-biased stencil for all spatial derivatives in one stage, and a backward-biased stencil in the next stage. For numerical consistency, the metrics should be calculated using forward- or backward-biased stencils as well.

## Time-Dependent Grid Motion Terms

Even with the improved definition of the grid metrics given in Eq. (21), the time-dependent metric invariant in Eq. (10) is still nonzero for both two and three dimensions. To remedy this situation, Thomas and Lombard[3] proposed the geometric conservation law (GCL) for computations on moving grids. In the GCL method, the Jacobian is allowed to evolve in time by solving the equation

$$(1/J)_t + (\xi_t/J)_\xi + (\eta_t/J)_\eta + (\zeta_t/J)_\zeta = 0 \tag{23}$$

To illustrate the problem, we look at the two-dimensional unsteady metric invariant

$$(1/J)_t + (\xi_t/J)_\xi + (\eta_t/J)_\eta = 0 \tag{24}$$

When we substitute in, we get

$$(x_\xi y_\eta - x_\eta y_\xi)_t + (-x_t y_\eta + y_t x_\eta)_\xi + (x_t y_\xi - y_t x_\xi)_\eta = 0 \tag{25}$$

Analytically, this is true. Numerically, however, this becomes

$$(x_\xi y_\eta)_t - (x_\eta y_\xi)_t + (x_\eta y_t)_\xi - (x_t y_\eta)_\xi + (x_t y_\xi)_\eta - (x_\xi y_t)_\eta \neq 0 \tag{26}$$

due to the numerical failure of the product rule.

Now let us write the Jacobian and unsteady metrics in this analytically equivalent form:

$$\begin{aligned}
\frac{1}{J} &= \frac{1}{2}\left[\left(x\frac{\xi_x}{J} + y\frac{\xi_y}{J}\right)_\xi + \left(x\frac{\eta_x}{J} + y\frac{\eta_y}{J}\right)_\eta\right] \\
\frac{\xi_t}{J} &= \frac{1}{2}\left[-\left(x\frac{\xi_x}{J} + y\frac{\xi_y}{J}\right)_t + (xy_t - x_t y)_\eta\right] \\
\frac{\eta_t}{J} &= \frac{1}{2}\left[-\left(x\frac{\eta_x}{J} + y\frac{\eta_y}{J}\right)_t - (xy_t - x_t y)_\xi\right]
\end{aligned} \tag{27}$$

Substituting into Eq. (24) again, we get

$$\begin{aligned}
&\left(\frac{1}{J}\right)_t + \left(\frac{\xi_t}{J}\right)_\xi + \left(\frac{\eta_t}{J}\right)_\eta \\
&\quad = \frac{1}{2}\left[\left(x\frac{\xi_x}{J} + y\frac{\xi_y}{J}\right)_{\xi t} + \left(x\frac{\eta_x}{J} + y\frac{\eta_y}{J}\right)_{\eta t}\right] \\
&\quad + \frac{1}{2}\left[-\left(x\frac{\xi_x}{J} + y\frac{\xi_y}{J}\right)_{t\xi} + (xy_t - x_t y)_{\eta\xi}\right] \\
&\quad + \frac{1}{2}\left[-\left(x\frac{\eta_x}{J} + y\frac{\eta_y}{J}\right)_{t\eta} - (xy_t - x_t y)_{\xi\eta}\right]
\end{aligned} \tag{28}$$

which is analytically and numerically zero if

$$(x)_{\xi t} = (x)_{t\xi} \tag{29}$$

Equation (29) is true for time-marching schemes that can be written in the form of Eq. (17), such as the Adams–Bashforth scheme. Also, Eq. (29) holds for Runge–Kutta time-marching schemes because each stage can be written in the form of Eq. (17). This will also work for MacCormack-type schemes, so long as the metrics are computed using the same biased stencils used in the spatial differences at each stage.

The three-dimensional Jacobian and unsteady metrics have a similar form:

$$\begin{aligned}
\frac{1}{J} &= \frac{1}{3}\left[\left(x\frac{\xi_x}{J} + y\frac{\xi_y}{J} + z\frac{\xi_z}{J}\right)_\xi + \left(x\frac{\eta_x}{J} + y\frac{\eta_y}{J} + z\frac{\eta_z}{J}\right)_\eta \right. \\
&\quad \left. + \left(x\frac{\zeta_x}{J} + y\frac{\zeta_y}{J} + z\frac{\zeta_z}{J}\right)_\zeta\right]
\end{aligned} \tag{30}$$

$$\begin{aligned}
\frac{\xi_t}{J} &= \frac{1}{3}\left(-\left(x\frac{\xi_x}{J} + y\frac{\xi_y}{J} + z\frac{\xi_z}{J}\right)_t + \{x[(y_t z)_\zeta - (y_\zeta z)_t] + y[(x_\zeta z)_t \right. \\
&\quad - (x_t z)_\zeta] + z[(x_t y)_\zeta - (x_\zeta y)_t]\}_\eta - \{x[(y_t z)_\eta - (y_\eta z)_t] \\
&\quad \left. + y[(x_\eta z)_t - (x_t z)_\eta] + z[(x_t y)_\eta - (x_\eta y)_t]\}_\zeta\right)
\end{aligned} \tag{31}$$

$$\begin{aligned}
\frac{\eta_t}{J} &= \frac{1}{3}\left(-\left(x\frac{\eta_x}{J} + y\frac{\eta_y}{J} + z\frac{\eta_z}{J}\right)_t - \{x[(y_t z)_\zeta - (y_\zeta z)_t] + y[(x_\zeta z)_t \right. \\
&\quad - (x_t z)_\zeta] + z[(x_t y)_\zeta - (x_\zeta y)_t]\}_\xi + \{x[(y_t z)_\xi - (y_\xi z)_t] \\
&\quad \left. + y[(x_\xi z)_t - (x_t z)_\xi] + z[(x_t y)_\xi - (x_\xi y)_t]\}_\zeta\right)
\end{aligned} \tag{32}$$

$$\frac{\zeta_t}{J} = \frac{1}{3}\left(-\left(x\frac{\zeta_x}{J} + y\frac{\zeta_y}{J} + z\frac{\zeta_z}{J}\right)_t + \{x[(y_t z)_\eta - (y_\eta z)_t] + y[(x_\eta z)_t - (x_t z)_\eta] + z[(x_t y)_\eta - (x_\eta y)_t]\}_\xi - \{x[(y_t z)_\xi - (y_\xi z)_t] + y[(x_\xi z)_t - (x_t z)_\xi] + z[(x_t y)_\xi - (x_\xi y)_t]\}_\eta\right) \quad (33)$$

## Calculation of the Grid Metrics

At first glance, this new method of calculating the metrics does not look appealing because the work involved in obtaining the new metrics is much greater than that of the original metrics. In this section, the strategy for computing the unsteady metrics for a Runge–Kutta-type scheme is developed as an example.

It is assumed that the grid motion is known at the start of each Runge–Kutta stage, either from body motion or from a grid adaption process. Thus, we know the grid coordinates $x$, $y$, and $z$ at both the beginning (time level $l$) and end of the stage (time level $l+1$).

At this point, the instantaneous grid metrics and Jacobian can be calculated at the $l$ and $l+1$ time levels (noting that, as we march in time, the $l+1$ level becomes the $l$ level at the next stage, saving this part of the computation at the cost of storing two levels of grid metrics). From these, the time derivatives of the grid metrics can be calculated and the unsteady grid metrics are computed. Note that analytic time derivatives must not be used; these will cause the same type of errors as have been reported from the use of analytic grid metrics.

## Numerical Scheme

The numerical scheme used for the test cases is a sixth-order compact scheme using a multistage optimized Runge–Kutta time-stepping method. The reason for choosing this scheme is that it will illustrate the effectiveness of the proposed metrics for large-stencil high-order schemes, which have historically had problems due to inconsistent metric specification.

The numerical scheme uses the Hixon prefactored sixth-order compact scheme[9] for the spatial differences. The time marching uses the Stanescu and Habashi[10] fourth-order nonlinear low storage extension of the Hu et al.[11] 5–6 low dispersion and dissipation Runge–Kutta method. To remove unresolved waves, the conserved variables are filtered at every time level using the explicit 10th-order filter of Kennedy and Carpenter.[12] Because the form of the numerical scheme is not the focus of this work, the reader is referred to Refs. 9, 13, and 14 for a full description of the scheme and its previous applications.

## Numerical Test Problem

The test problem chosen is that of a three-dimensional combined acoustic and entropy pulse propagating through a three dimensionally time-varying grid. To ensure that boundary condition errors will not be present, all boundaries in the domain will be periodic. However, for efficiency, an 11-point explicit stencil is used for the differences at the grid boundaries.[9] For comparative purposes, the same problem is run using the strong conservation equations on a uniform, motionless grid. The solutions from the moving grid are then compared to this reference solution to determine the effects of the equation formulation on the accuracy of the solution.

### Computational Grid

The computational grid uses $31 \times 41 \times 61$ points. The grid is given by

$$\begin{aligned} x &= 0.1\xi - (0.1/\pi)\sin[(2\pi/10)\xi + (2\pi/20)\eta + (2\pi/30)\zeta]\sin(2\pi t) \\ y &= 0.1\eta - (0.1/\pi)\sin[(2\pi/15)\xi + (2\pi/10)\eta + (2\pi/60)\zeta]\sin(4\pi t) \\ z &= 0.1\zeta - (0.1/\pi)\sin[(2\pi/30)\xi + (2\pi/40)\eta + (2\pi/15)\zeta]\sin(6\pi t) \end{aligned} \quad (34)$$

In these grids, the minimum spacing in any direction is 0.03183, whereas the maximum spacing is 0.1682. Notice that there are at least 10 points per wavelength in these calculations. Because the sixth-order compact scheme is capable of resolving waves with as little as six points per wavelength, any grid metric problems are not due to inadequate resolution.

### Three-Dimensional Convection and Propagation

In this problem, a three-dimensional combined acoustic and entropy pulse in a uniform mean flow is set as the initial condition, and its propagation outward and convection downstream is computed. The initial conditions are

$$\begin{aligned} \rho(x,y,z,0) &= 1.0 + A\exp\left\{\frac{-\ln(2)}{(0.4)^2}[(x-1.5)^2 + (y-2.0)^2 + (z-3.0)^2]\right\} \\ u(x,y,z,0) &= 0.5, \qquad v(x,y,z,0) = 0.0, \qquad w(x,y,z,0) = 0.0 \\ p(x,y,z,0) &= \left(\frac{1.0}{\gamma}\right) + A\exp\left\{\frac{-\ln(2)}{(0.4)^2}[(x-1.5)^2 + (y-2.0)^2 + (z-3.0)^2]\right\} \end{aligned} \quad (35)$$

Two cases are chosen to test the effect of the metrics on the linear and nonlinear performance of the numerical scheme. For the linear case, $A$ is $1.0e{-}3$; for the nonlinear case, $A = 1.0$. In all cases, the time step $\Delta t = 0.02$.

## Results

### Grid Motion

In all numerical tests, the grid motion is identical and given in Eq. (34). Figure 1 shows the time history of the grid on the $\zeta = 31$ plane. Figure 2 shows the time history of the maximum Jacobian in the grid, whereas Fig. 3 shows the time history of the maximum unsteady grid metrics. Note that, although there are two different ways to compute these terms, the actual numerical difference is relatively small (about 2% at most). Thus, the metrics shown are computed using Eqs. (30–33).

### Linear Propagation and Convection

Figure 4 shows the density contours on the $z = 3$ plane at time $= 1.0$ for the reference solution and the three methods tested. For all methods except the strong conservation method with standard metrics, the solution is very reasonable, with a very good comparison between the chain rule and strong conservation methods. Note how the error due to the inconsistent unsteady metrics ruins the solution for the strong conservative method using the standard unsteady metrics.

Figure 5 compares the density results at time $= 1.0$ on the $y = 2$, $z = 3$ line from the three methods with the solution from the stationary grid. Notice that both the chain rule solution and the strong conservation solution using the new unsteady metrics obtain a good quantitative solution, whereas the error from the strong conservation method using the old unsteady metrics overwhelms the density wave.

Figure 6 shows the magnitude of the density error at time $= 1.0$ on the $y = 2$, $z = 3$ line between the three methods using the stationary grid solution as the reference. Both the strong conservation form with new metrics and the chain-rule form with old metrics return equivalent solutions, with two orders of magnitude less error than the strong conservation form using the old unsteady metrics.

Note that, for computational acoustics, the waves to be propagated can be very small with regard to the mean flow values; thus, the errors from the unsteady metrics shown in Figs. 4 and 6 are unacceptable for this type of calculation.

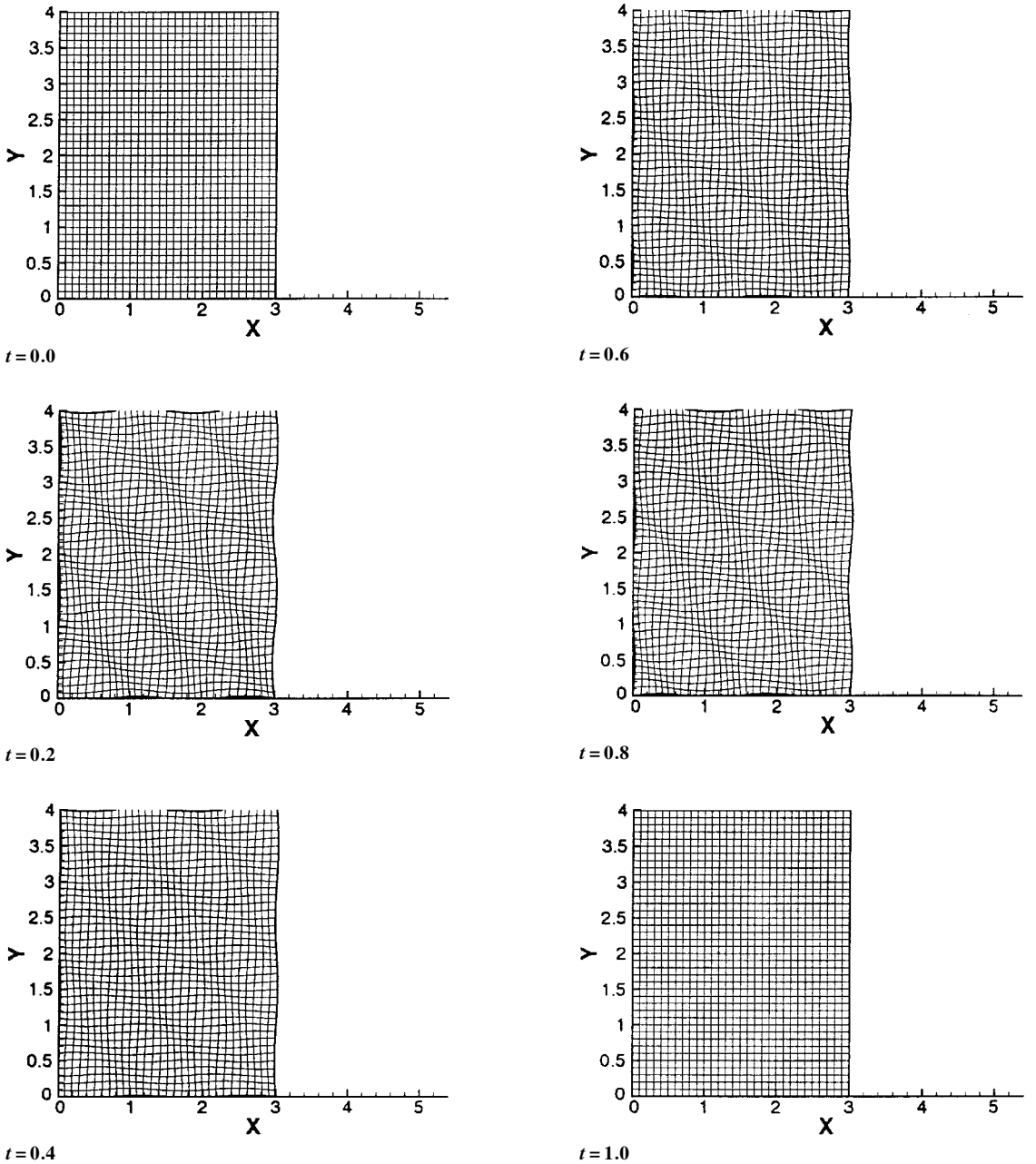


**Fig. 1 Grid history on $z = 3$ plane.**

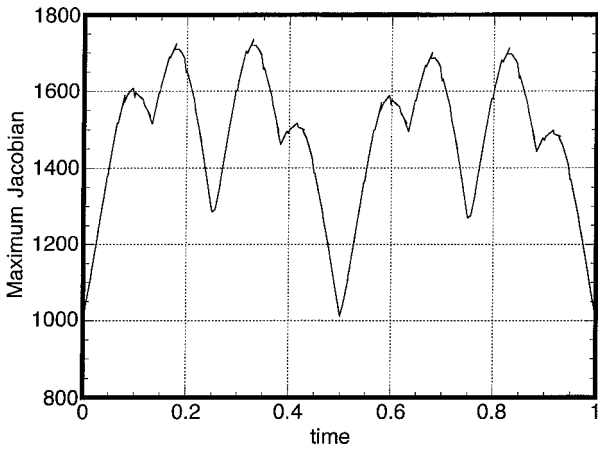


**Fig. 2 Time history of maximum Jacobian.**

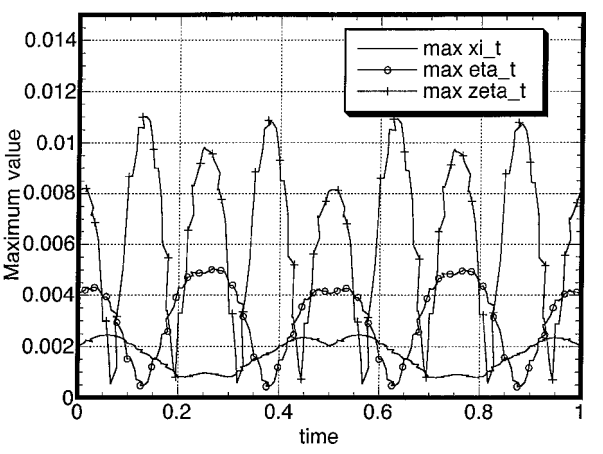


**Fig. 3 Time history of maximum unsteady grid metrics.**

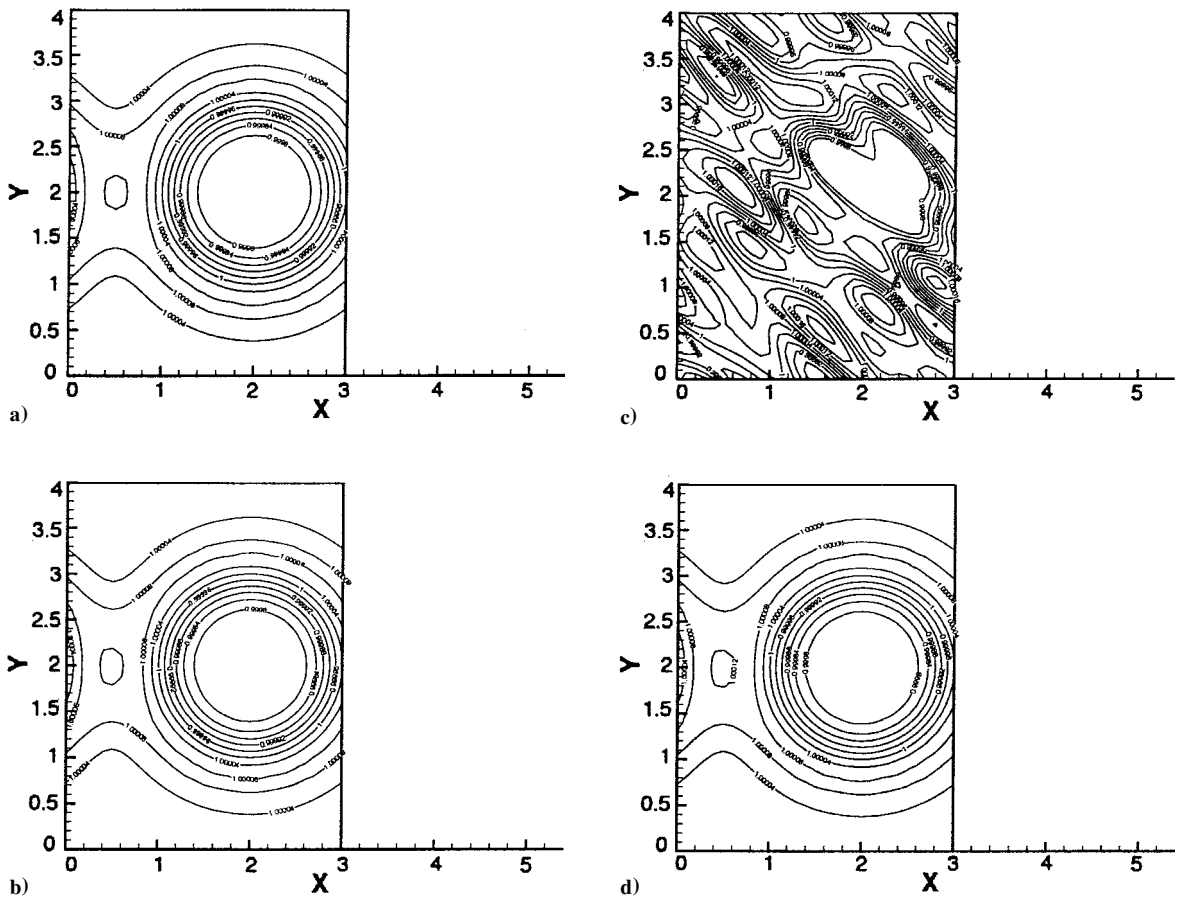


**Fig. 4 Comparison of density contours on $z = 3$ plane at time = 1.0 for linear test problem: a) strong conservation on stationary grid, b) chain rule on moving grid, c) strong conservation with standard unsteady metrics on moving grid, and d) strong conservation with consistent unsteady metrics on moving grid.**

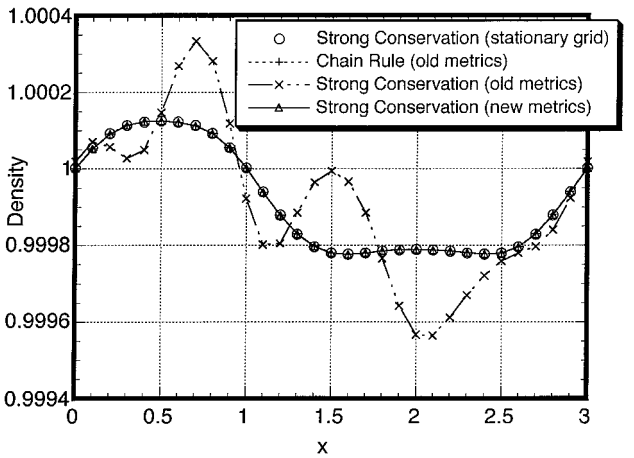


**Fig. 5 Density along $y = 2$, $z = 3$ line for linear test problem at $t = 1.0$.**

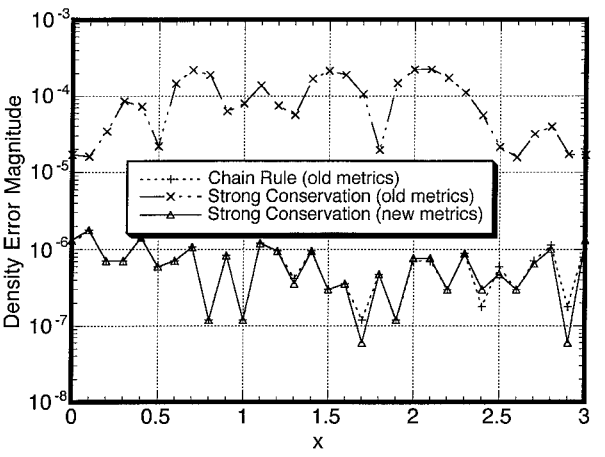


**Fig. 6 Density error magnitude along $y = 2$, $z = 3$ line for linear test problem at $t = 1.0$.**

### Nonlinear Propagation and Convection

Figure 7 shows the density contours for the nonlinear test problem on the $z = 3$ plane at time = 1.0 for the reference solution and the three methods tested. In this case, the results from all three methods are very comparable to the stationary grid solution.

Figure 8 compares the density results at time = 1.0 on the $y = 2$, $z = 3$ line from the three methods with the solution from the stationary grid for the high-amplitude case. In this case, all three solutions are comparable. Figure 9 shows the magnitude of the density error at time = 1.0 on the $y = 2$, $z = 3$ line between the three methods and the stationary grid calculation. From Figs. 8 and 9, it is shown that the effect of metric error becomes much smaller with higher-amplitude waves.

It is theorized that there are two reasons for this. First, the amplitude of the grid metric error is not changing very much as compared to the amplitude of the pulse. To illustrate, the pulse amplitude changes by a factor of 1000, whereas the metric error (which is related to the total magnitude) would change by a factor of 2. Second, the grid motion may be causing spatial resolution problems for all three methods, overshadowing any grid metric contributions. To illustrate this, note the greatly reduced width of the density pulse in Fig. 8 compared to Fig. 5. Figures 7–9 show that all methods return equivalent answers for this nonlinear test problem. However, note that the metric errors will still have a great effect on low-amplitude waves.

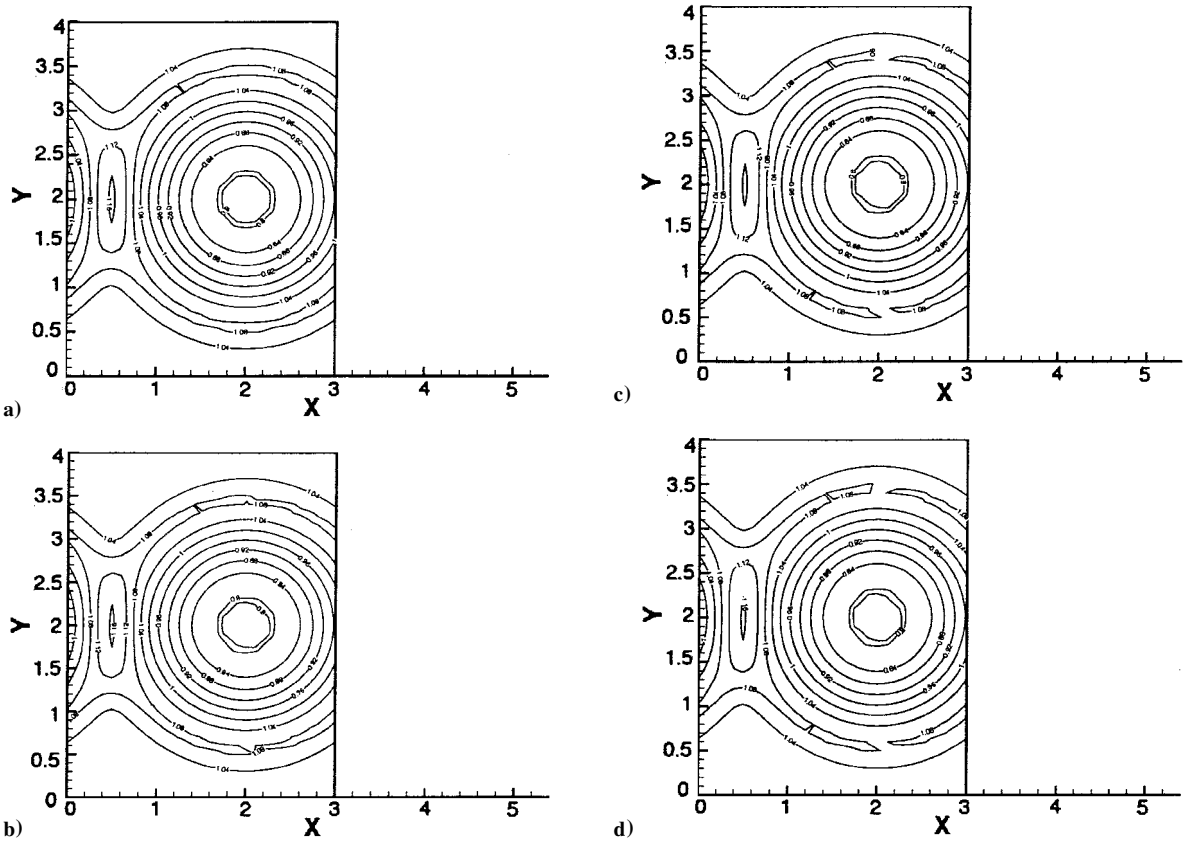


**Fig. 7 Comparison of density contours on $z = 3$ plane at time = 1.0 for nonlinear test problem: a) strong conservation on stationary grid, b) chain rule on moving grid, c) strong conservation with standard unsteady metrics on moving grid, and d) strong conservation with consistent unsteady metrics on moving grid.**

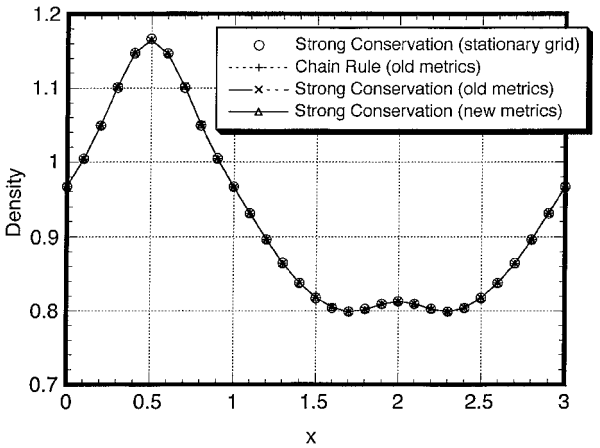


**Fig. 8 Density along $y = 2$, $z = 3$ line for nonlinear test problem at $t = 1.0$.**

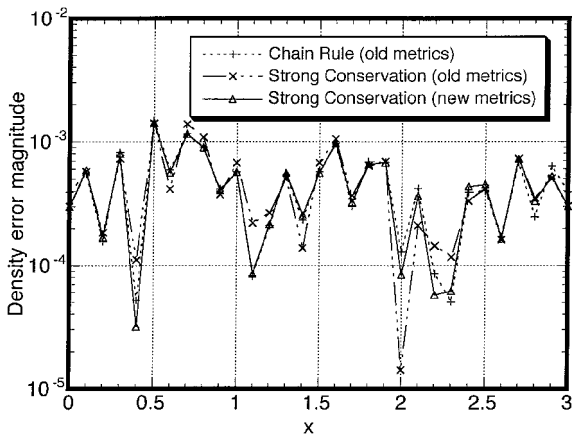


**Fig. 9 Density error magnitude along $y = 2, z = 3$ line for nonlinear test problem at $t = 1.0$.**

## Conclusions

A new form of the unsteady grid metrics and a Jacobian for the strong conservation equations were derived and tested for a three dimensionally moving grid. This new method eliminates numerical inconsistencies from the unsteady metrics by making them exactly satisfy the invariants of the transformation. By doing this, a numerically consistent and strongly conservative method is derived for finite differencing schemes of any order. This method proved to be as accurate as the chain-rule form of the equations, which has no numerical constraints on the form of the metrics. Note that for all tests run, the chain-rule form of the equations returned equally accurate solutions. However, for highly nonlinear problems, the strong conservation form will give the correct jumps across flow and grid discontinuities whereas the chain-rule form, being numerically nonconservative, may not.

## Acknowledgments

This work was conducted under Grant NCC3-531 with the NASA John H. Glenn Research Center at Lewis Field. L. A. Povinelli was the Technical Monitor. The author would like to thank Reda Mankbadi for his many informative discussions and suggestions about this work.

## References

[1] Vinokur, M., "Conservation Equations of Gasdynamics in Curvilinear Coordinate Systems," *Journal of Computational Physics*, Vol. 14, No. 2, 1974, pp. 105–125.

[2] Pulliam, T. H., and Steger, J. L., "Implicit Finite Difference Simulations of Three-Dimensional Compressible Flow," *AIAA Journal*, Vol. 18, No. 2, 1980, pp. 159–167.

[3] Thomas, P. D., and Lombard, C. K., "Geometric Conservation Law and Its Application to Flow Computations on Moving Grids," *AIAA Journal*, Vol. 17, No. 10, 1979, pp. 1030–1037.

[4] Hindman, R. G., "Generalized Coordinate Forms of Governing Fluid Equations and Associated Geometrically Induced Errors," *AIAA Journal*, Vol. 20, No. 10, 1982, pp. 1359–1367.

[5] Hixon, R., Shih, S.-H., Dong, T., and Mankbadi, R. R., "Evaluation of Generalized Curvilinear Coordinate Transformations Applied to High-Accuracy Finite Difference Schemes," AIAA Paper 98-0370, Jan. 1998.

[6]Tam, C. K. W., and Webb, J. C., "Dispersion-Relation-Preserving Finite Difference Schemes for Computational Acoustics," *Journal of Computational Physics*, Vol. 107, No. 2, 1993, pp. 262–281.

[7]Gaitonde, D. V., and Visbal, M. R., "Further Development of a Navier–Stokes Solution Procedure Based on Higher-Order Formulas," AIAA Paper 99-0557, Jan. 1999.

[8]Pulliam, T. H., "Euler and Thin Layer Navier–Stokes Codes: ARC2D and ARC3D," *Computational Fluid Dynamics Users Workshop*, Univ. of Tennessee Space Inst., Tullahoma, TN, 1984.

[9]Hixon, R., "A New Class of Compact Schemes," AIAA Paper 98-0367, 1998.

[10]Stanescu, D., and Habashi, W. G., "2N-Storage Low Dissipation and Dispersion Runge–Kutta Scheme for Computational Acoustics," *Journal of Computational Physics*, Vol. 143, No. 2, 1998, pp. 674–681.

[11]Hu, F. Q., Hussaini, M. Y., and Manthey, J., "Low-Dissipation and -Dispersion Runge–Kutta Schemes for Computational Acoustics," *Journal of Computational Physics*, Vol. 124, No. 1, 1996, pp. 177–191.

[12]Kennedy, C. A., and Carpenter, M. H., "Several New Numerical Methods for Compressible Shear-Layer Simulations," *Applied Numerical Mathematics*, Vol. 14, No. 4, 1994, pp. 397–433.

[13]Hixon, R., Shih, S.-H., and Mankbadi, R. R., "Evaluation of Boundary Conditions for the Gust-Cascade Problem," *Journal of Propulsion and Power*, Vol. 16, No. 1, 2000, pp. 72–78.

[14]Hixon, R., Shih, S.-H., Mankbadi, R. R., and Scott, J. R., "Time Domain Solution of the Airfoil Gust Problem Using a High-Order Compact Scheme," AIAA Paper 98-3241, July 1998.

P. J. Morris
*Associate Editor*